Gamma irradiation-induced defects in borosilicate glasses for high-level radioactive waste immobilisation

RAUTIYAL, Prince, GUPTA, Gaurav, EDGE, Ruth, LEAY, Laura, DAUBNEY, Aaron, PATEL, Maulik, JONES, Alan and BINGHAM, Paul <http://orcid.org/0000-0001-6017-0798>

Published version

RAUTIYAL, Prince, GUPTA, Gaurav, EDGE, Ruth, LEAY, Laura, DAUBNEY, Aaron, PATEL, Maulik, JONES, Alan and BINGHAM, Paul (2020). Gamma irradiation-induced defects in borosilicate glasses for high-level radioactive waste immobilisation. Journal of Nuclear Materials.

Gamma irradiation-induced defects in borosilicate glasses for high-level radioactive waste immobilisation

P. Rautiyal [a*], G. Gupta [a], R. Edge [b], L. Leay [b], A. Daubney [b], M. K. Patel [c], A. H. Jones [a] and P. A. Bingham [a]

[a] *Materials and Engineering Research Institute, Sheffield Hallam University, City Campus, Howard Street, Sheffield S1 1WB, UK*

[b] *The University of Manchester, Dalton Cumbrian Facility, Westlakes Science and Technology Park, Moor Row, Cumbria CA24 3HA, UK*

[c] *The School of Mechanical, Aerospace and Civil Engineering, University of Manchester, Oxford Road, Manchester M19 9PL, UK*

[d] *Department of Mechanical Materials and Aerospace, Harrison Hughes Building, Brownlow Hill, University of Liverpool, Liverpool L69 3GH, UK*

*Corresponding author: prince.rautiyal@student.shu.ac.uk, Tel: +447442448037, Address: City Campus, Howard Street, Harmer Building Level 2, Sheffield S1 1WB

Abstract

Gamma irradiation-induced defects at doses of 0.5 and 5 MGy were studied in lithium sodium-borosilicate (LiNaBSi) and sodium barium-borosilicate (NaBaBSi) glasses, used for high-level radioactive waste immobilisation in the UK and India, respectively. X-band electron paramagnetic resonance (EPR), Raman and UV-Vis-nIR spectroscopies were used to characterise the glasses before and after irradiation. EPR and UV-Vis-nIR absorption spectroscopies revealed the formation of boron-oxygen hole centres (BOHC), electrons trapped at alkali cations or ET centres and peroxy-radicals (PORs) as defects common to both glasses. In addition, E^- or polaron centres were observed in NaBaBSi glasses, possibly related to formation of elemental sodium colloids. Time-dependent thermal annealing at a range of temperatures, including those relevant to canister centreline cooling (CCC), which may be of relevance to geological disposal in future technical assessments, was carried out to study thermal stability of these radiation-induced defects. It was observed that PORs are the most thermally-stable defects in both glasses. The influence of glass composition on the segregation of sodium; possible formation of metal colloids upon irradiation has been discussed.

1. Introduction

High-level radioactive waste (HLW) arises as a by-product from the reprocessing (extraction of unused fissile U and Pu) of spent nuclear fuel. HLW contains ~95% of the radioactivity of all the nuclear waste [1][2][3][4][5][6]. It consists of fission products (e.g. ^{90}Sr,^{137}Cs), transuranic elements or minor actinides (e.g. ^{237}Np, ^{241,243}Am, ^{244,245}Cm), corrosion products from reprocessing, cladding material (e.g. Fe, Ni, Cr, Tc, Mo, Zr) and process additives from reprocessing (e.g. Na, K, Li, Ca, Mg, Fe, S, F, Cl) [1][7][3][8][9]. This HLW is immobilized by vitrification in many countries including USA, France, UK, India, Japan, China, Russia, and S. Korea [1][4][10]. Following vitrification, the resulting wasteforms are stored safely above-ground, prior to their planned ultimate disposal in geological repositories. Understanding the long-term performance and stability of these radioactive wasteforms is thus vital to underpinning the provision of robust disposal safety cases to meet both regulatory and public safety concerns.

Whilst the long-term chemical durability of HLW wasteforms in simulated geological repository conditions has received, and continues to receive, considerable attention, the effects of self-irradiation of wasteforms have, to date, received less consideration. HLW wasteforms will experience radiation-induced structural changes due to β/γ-decay of fission products and α-decay of actinides over periods of time consistent with interim storage and geological disposal [1][3][11][12].

Fission products such as ^{90}Sr and ^{137}Cs undergo β/γ-decay that produces energetic β-particles, low-energy recoil nuclei and γ-rays. Interaction of these radiations with the wasteforms in which they are present will be the principal sources of heat generation and accumulated damage for the first few hundred years (~500) of storage and geological disposal, due to their associated short half-lives ($t_{1/2}$ ^{137}Cs = 30.2 years and $t_{1/2}$ ^{90}Sr = 28.8 years) [11][14]. Over geological disposal periods α-decay of minor actinides such as ^{240}Pu,^{241},^{243}Am, ^{237}Np and ^{244}Cm will be principally responsible for radiation damage, due to their long half-lives (≈10^6 years) [3][7][8][12][13].

The radiation damage effects can be placed into two main categories: ballistic (displacement of atom(s) in the glass network upon ballistic collision) and electronic (ionization processes, producing electron-hole pairs). Transmutation of fission

products upon radioactive decay can also change valences and atomic radii, but glass wasteforms have been shown to be capable of accommodating such changes [1][7][14].

Since the glass matrix will experience radiation effects mainly due to ionization from β/γ-decay during the first few hundred (~500) years, it becomes imperative to study these effects on the glass matrices [3][13][15]. To perform such studies, two approaches have been widely used on simulated, inactive glass samples: (i) irradiation with a high-flux electron beam using a TEM/SEM or using an electron beam in an accelerator facility [13][16][17]; and (ii) irradiation using ^{60}Co or ^{137}Cs sources [13][15]. TEM/SEM can simulate doses of ~1 GGy in less than one minute but the irradiation depth that can be accessed is very small, from a few hundred nanometres to micrometres; and these are mainly surface effects [15]. Moreover, a large proportion of the incident electrons simply pass through the sample and hence calculated “doses” can be misleading [18][19]. Using radioactive sources such as ^{60}Co or ^{137}Cs can enable bulk irradiated samples to be obtained, but achieving doses of a few MGy requires long irradiation times (~10 days for 5 MGy with dose rate of 350 Gy/min, as in the present case), however, they offer realistic simulations of dose rates. Bulk irradiated samples enable the use of a wider range of characterisation techniques (e.g. EPR, NMR, Raman spectroscopies) to study defects and structural changes in glass matrices [3][13][20].

Radiation interaction mechanisms are complex and depend on the nature and dose of the radiation, glass structure, glass composition (glass forming and modifying species), bonding and thermal history of the glass [21]. Radiation-induced microstructural defects / changes can enable the migration of charge compensators and other atoms under the induced electric field, formation of clusters of alkalis, and / or formation of molecular oxygen [17][22]. Any changes in the (nano, micro) structure of glass wasteforms due to the radiation arising from the decay of radionuclides present in the HLW therein, can translate into changes in the micro- and macroscopic properties of the wasteform.

In simple alkali silicate glasses, alkalis act as network modifiers, depolymerising the ≡Si-O-Si≡ network and introducing non-bridging oxygens (NBOs). In silicate glasses more generally, the distribution of NBOs depends on the nature of the

modifier cations, their abundance and their cationic field strength, and nanoscale inhomogeneity can exist in such glasses [23]. Early work by Yun *et al*. [24] and Dell *et al.* [25] used ^{11}B “wide-line” nuclear magnetic resonance (NMR) spectroscopy to study the short-range structure of sodium borosilicate glasses. Followed by many advancements in spectroscopy, more recent studies have led to models which can explain the role of alkalis as charge compensators (via conversion of BO_3 to BO_4 units) or as network modifiers (forming NBOs), variations in the structure based on their type and content, changes due to the composition, and degree of Si/B mixing associated with bridging oxygens (BOs) and NBOs [26][27][28][29]. In borosilicate glasses the mixing of network-forming structural units (Si/B mixing), the distribution and mixing of modifying species (e.g. alkalis and alkaline earths), and their role in the glass network are critical factors that determine the mechanical strength, physical properties and chemical durability of the glass [29]. In a mixed-alkali borosilicate glass, the distribution of alkalis and the degree of Si/B mixing is even more complicated. In mono- and mixed-alkali borosilicate glasses investigated by Du and Stebbins [27][29] using 3Q-MAS (triple-quantum magic angle spinning) ^{11}B and ^{17}O NMR, it was shown that there is significant heterogeneity in Li-borosilicate glass in comparison with Na- and K- containing borosilicate glasses. They reported significant heterogeneity in terms of Si/B mixing for mixed Li-Na and Li-K glasses, as indicated by a lower fraction of tetrahedral boron (BO_4), Si-O-B and higher fraction of NBOs. They suggested that heterogeneity increases with increasing cationic field strength, and NBOs are more likely to associate with smaller alkalis. In alkali-alkaline earth (Na-Ba) borosilicate glass, Mishra *et al.* [30] suggested that sodium acts as a charge compensator when Na/B > 0.5, facilitating increased Si/B mixing by charge-compensating BO_4 units. The formation of NBOs was attributed to breaking of Si-O-Si and Si-O-B bonds with increasing Na^+ concentration. The Na^+ ions occupy sites close to BO_4^- units, while Ba^{2+} ions occupy sites less close to NBOs and have more modest interaction with silicon or boron structural units [30][31][32].

The primary aim of this study was to contribute to developing greater fundamental understanding of the nature of gamma irradiation-induced defects in two simple (4-oxide) representative HLW host (base) glasses at two different doses (0.5 MGy / low and 5 MGy / high) using a multi-spectroscopic approach including EPR, UV-Vis-nIR optical absorption and Raman spectroscopies. Further aims of this

research included determining how or whether the radiation-induced defect types and abundances differed between the two base glasses (thereby providing information on glass compositional effects). Also, this study aims to uncover the mechanisms of creation of radiation-induced defects (e.g. nano/micro structural changes which were not present in un-irradiated glasses); and an examination of the underlying gamma irradiation-induced defect centres which are accessed / annihilated / recombined upon thermal annealing and hence their stability as functions of temperature and time. Meeting these aims has thereby provided new insight into longer-term interim storage and geological repository behaviour of UK and Indian HLW wasteforms.

2. Experimental Procedures

Bulk samples of UK glass, Li_2O-Na_2O-B_2O_3-SiO_2 (LiNaBSi) [2] and Indian glass, Na_2O-BaO-B_2O_3-SiO_2 (NaBaBSi) [33] were fabricated using a standard melt-quench-anneal method. High purity (≥99.9%) sand (SiO_2), sodium carbonate (Na_2CO_3), lithium carbonate (Li_2CO_3), barium carbonate ($BaCO_3$) and boric acid (H_3BO_3) were used to fabricate these glasses. Nominal compositions (mol%) of the oxide glasses are given in Table 1. All raw materials except boric acid (H_3BO_3), which begins to decompose at temperatures well below 100 ˚C, were dried, prior to weighing and mixing, in an electric oven at 110 ˚C for 24 hours. After weighing using a 3 decimal-place balance into polymeric sample bags, batches to produce 200 grammes of glass were mixed thoroughly for 3-5 minutes to attain good mixing. The LiNaBSi and NaBaBSi glass raw material mixtures were placed in recrystallized Al_2O_3 crucibles and then heated in air at 5 ˚C / minute to 1150 ˚C (LiNaBSi glass) or 1050 ˚C (NaBaBSi glass). The molten glasses were held at these respective temperatures for 2 h and then poured onto a steel mould to form discs. These discs were cooled slightly then removed from the moulds and annealed at temperatures just below their glass transition temperatures (T_g) at 480 ˚C for 2 h in an electric furnace, then cooled slowly to room temperature. Samples of all glasses were then ground to a 15 μm surface finish using SiC pads, then polished using an aqueous suspension of CeO_2 to obtain a smooth, mirror-polished surface to <1 μm.

Table 1. Nominal glass compositions (mol%)

Glass	SiO_2	Na_2O	B_2O_3	Li_2O	BaO

NaBaBSi	41.67	21.83	20.83	-	15.62
LiNaBSi	60.50	10.49	18.50	10.50	-

To assess the amorphous nature of the as-fabricated glass samples, X-ray diffraction (XRD) measurements were performed using an X-Pert Pro diffractometer equipped with a monochromated Cu-$K_{\alpha 1}$ X-ray source and a PIXcel 3D detector. Data collections were performed in theta-theta geometry in the 2θ range of 10-70° with a step size of 0.016°. Figure S1 (Supplementary Information) shows the X-ray diffraction patterns for the LiNaBSi and NaBaBSi glasses. The presence of only amorphous humps and no sharp peaks confirms that both glasses were X-ray amorphous.

The irradiations were performed using a Foss Therapy Services 812 ^{60}Co Gamma irradiator at the Dalton Cumbrian Facility, The University of Manchester, which supplies 1.17-1.33 MeV energy gamma photons [34]. The samples were irradiated with doses of 0.5 and 5 MGy. Absorption of the gamma rays by the Pb walls of the irradiator means that the temperature in the irradiator chamber reaches approximately 314 K over the first 45 minutes of each irradiation and, thereafter, remains stable. The irradiator has gamma sources which can supply absorbed dose rates of 0.5 to 350 Gy/min. The absorbed dose rates at the centre of each sample were determined by replacing each sample with a high-dose rate ionization chamber, model name 10x6-0.18, and Accu-Dose+ base unit, both supplied by Radcal. To perform annealing studies sister samples were irradiated with equivalent doses. Thermal annealing of irradiated glasses was performed using a temperature-calibrated electric oven at 5 different temperatures between 373 K and 773 K for 16 and 24 hours. In total 40 specimens were synthesised, irradiated, and annealed.

Raman spectroscopic measurements were carried out to study changes in the coordination chemistry of glass constituent units. These measurements were performed using a Thermo Scientific DXR2 Raman imaging microscope equipped with a 10 mW 532 nm laser. Raman spectra were acquired in the range of 100-2000 cm^{-1} using a CCD detector and grating set to 900 lines / mm. The background signal was corrected using the software package Omnic, and temperature and excitation line effects were corrected using a method adapted from Long [35] and the data was normalised to the highest peak at ~1050 cm^{-1}. A 50x objective lens and 50 μm aperture was used for an optimum focus. The in-built software package OMNIC was

used for data acquisition and to perform background corrections. To obtain higher S/N ratios, 30 accumulations of 15 seconds each were acquired.

First-derivative continuous wave monolithic sample EPR spectra were recorded for all glass samples at room temperature using an X-band frequency of ~ 9.6 GHz and a sweep width and centre field of 370 and 250 mT, respectively, using a Bruker EMXnano EPR spectrometer. The magnetic field modulation used was 100 kHz. The microwave power used was 0.3162 mW and modulation amplitude was 0.4 mT. Experimental *g*-values were calculated using the formula $h\nu = g\beta H$, where h is Planck's constant, H is the applied magnetic field measured at the centre of resonance, ν is the spectrometer frequency and β is the Bohr magneton. Second-derivative EPR spectra were obtained by differentiating the first-derivative EPR data to further elucidate the complex resonance absorption signal arising due to the superimposition of resonances arising from different paramagnetic centres.

UV-Vis-nIR optical absorption spectroscopic measurements were obtained on flat, polished samples at room temperature using a Varian Cary 50 Scan spectrophotometer. The measurements were collected in the wavelength range of 190-1100 nm. Measurements were taken in absorption mode with a dual beam scan rate of 60 nm/min. The in-built software package, Scan, was used to correct the zero baseline. Data were corrected to a path length of 1 mm.

3. Results

3.1 Glass discoloration under irradiation

Changes in the visible coloration of the glasses following gamma-irradiation are illustrated in Table 2. The LiNaBSi glass, which was initially transparent and colourless, turned brown and the NaBaBSi glass, which was initially transparent and slightly yellow in colour, turned blue, following irradiation. Similar depths of visible coloration occurred in all glasses. The colour intensity is less pronounced in the images (Table 2) for the 0.5 MGy-irradiated samples due to differences in sample thickness (0.5 MGy 3 – 4 mm; and 5 MGy ~ 10 mm).

Table 2. Photographs showing the change in transparency and colour after γ-irradiation of LiNaBSi and NaBaBSi glasses. The thickness for pristine and 5 MGy dose glasses was 10 mm while that for 0.5 MGy dose glasses was 3 – 4 mm.

NaBaBSi Glass		
0 MGy (~ 10 mm)	**0.5 MGy (~3-4 mm)**	**5 MGy (~ 10 mm thick)**
	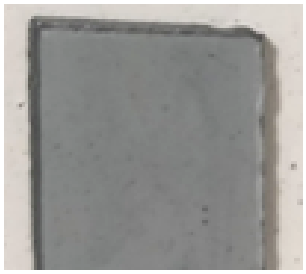	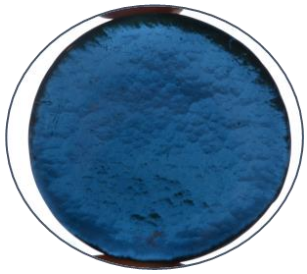
LiNaBSi Glass		
0 MGy (~ 10 mm)	**0.5 MGy (~3-4 mm)**	**5 MGy (~ 10 mm thick)**
		

Some of the colour changes are easier to observe in thicker samples, and with different lighting conditions.

3.2. Electron Paramagnetic Resonance Spectroscopy

Figure 1 shows the first-derivative X-band (~9.6 GHz) room temperature EPR spectra for pristine and irradiated NaBaBSi and LiNaBSi glass specimens. No EPR signals were detected in the unirradiated glasses. In the irradiated NaBaBSi glass a signal is identified with an experimental value of g~1.974 ± 0.002 and 1.972 ± 0.002 at 0.5 and 5 MGy, respectively, corresponding to a magnetic field of ~348 mT; whereas it is not present in the LiNaBSi glass. This is attributed to E^- or polaron centres (this defect is formed when an electron is trapped on a sodium cation, converting it into elemental sodium) [22][36][37]. An EPR signal centred at g~2.00 was detected in all irradiated glasses. For both the LiNaBSi and NaBaBSi glasses,

the identified EPR signal at g~2.00 is a four line (quartet) hyperfine structure. This signal is probably a convolution of signals due to different paramagnetic centres (g values are calculated using the magnetic field values at which the second derivative becomes negative, as in Figure 2). This has been attributable to boron-oxygen hole centres (BOHCs) [38][39][40][41]. A BOHC is defined as a hole trapped on the non-bridging oxygen (NBO) atom in a trigonal borate unit (=B-O•), formed by radiation-induced breaking of B-O-B bonds [41][42][43][44]. For the NaBaBSi glass, the signal at g ~1.991 has been attributed to ET centres, that are either F^+ centres or electrons trapped at cations [38][45]. For the LiNaBSi glass a weak isotropic signal at g~1.997 and 1.996, at 0.5 and 5 MGy respectively, can be attributed to the ET centres [38][45].

Figure 1. *Intensity-normalised first-derivative EPR spectra for pristine and irradiated LiNaBSi and NaBaBSi glasses showing various defect centres created after ^{60}Co γ-irradiations at 0.5 MGy and 5 MGy doses.*

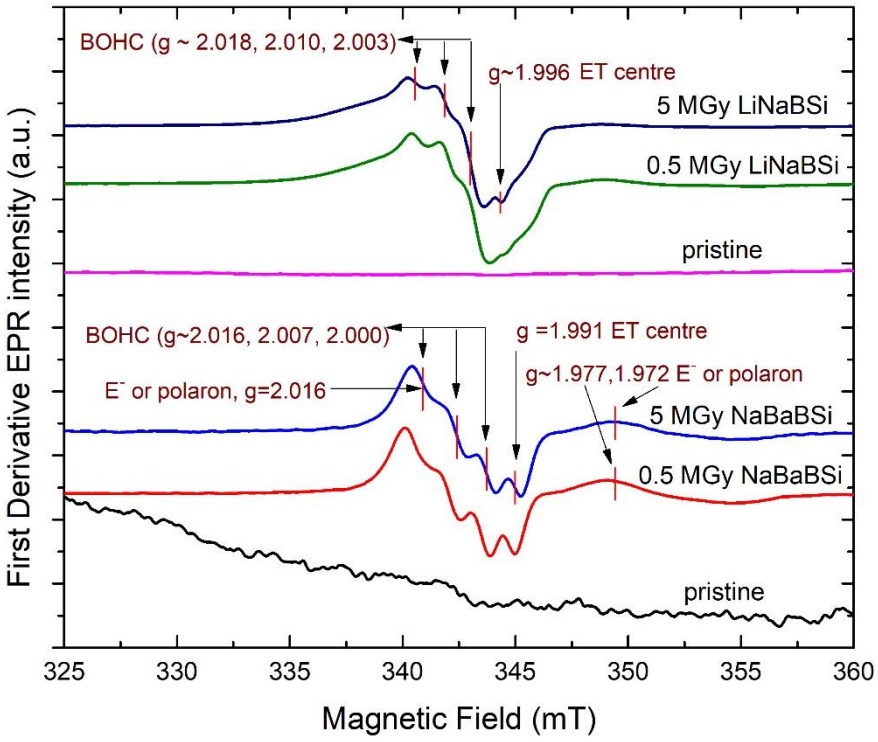

Figure 2 shows the second-derivative EPR spectra for both NaBaBSi and LiNaBSi glasses irradiated at 0.5 and 5 MGy. These were plotted to enhance definition and to further investigate any underlying signals due to radiation-induced paramagnetic defect centres. The four-line hyperfine (quartet) structure which has

been attributed to BOHCs, shown in the first-derivative plots (Figure 1), is slightly better resolved in the second-derivative plot for NaBaBSi glass, for both 0.5 and 5 MGy irradiated specimens (labelled only for 5 MGy). The signal at g~1.974 ± 0.002 and g ~1.972 ± 0.002, attributed to E^- centres, is also present in the second-derivate spectra. In addition, the improved definition reveals an isotropic signal at g~ 2.018 and 2.016 (at 0.5 and 5 MGy, respectively) with a linewidth in the range 1.4 - 1.5 mT, corresponding to a magnetic field of ~ 341 mT. This can also be attributed to the E^- centres responsible for formation of elemental sodium colloids [37][46][45]. The second-derivative EPR spectra for the LiNaBSi glass did not reveal any additional defect centres. The signal at g~1.997 and g~1.996 (at 0.5 and 5 MGy, respectively) is attributed to ET centres (Figure 3). The calculated experimental g-values and the corresponding defect types for the two glasses are given in Table 3.

Figure 2. *Intensity-normalised second-derivative EPR spectra for LiNaBSi and NaBaBSi glasses irradiated with 0.5 and 5 MGy ^{60}Co γ-radiation.*

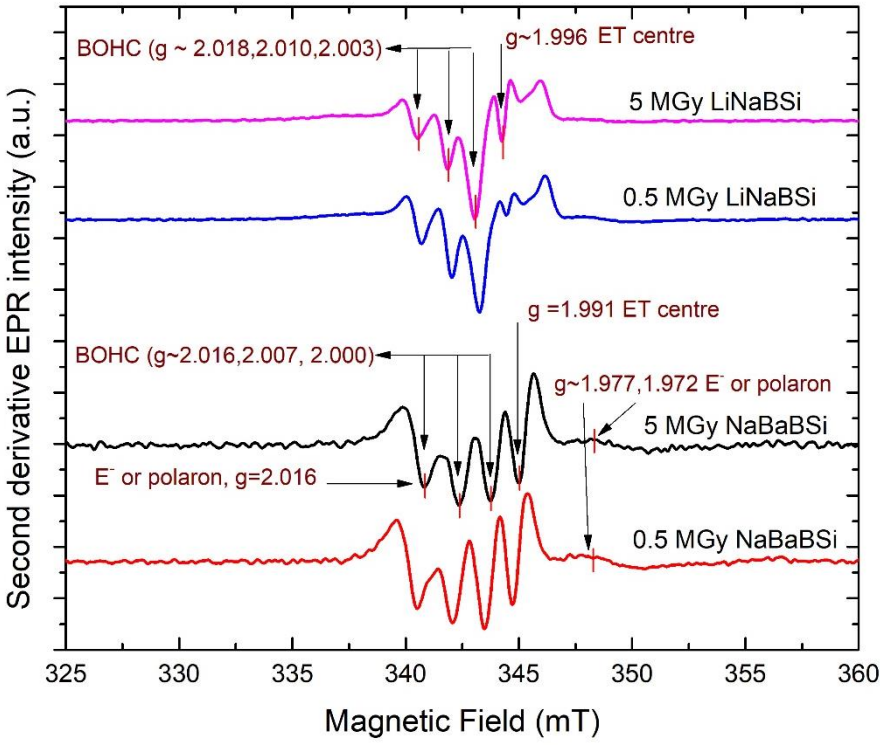

Table 3. *Experimental g-values and corresponding defect type for NaBaBSi and LiNaBSi glasses irradiated with 0.5 and 5 MGy ^{60}Co γ-radiation.*

NaBaBSi 0.5 MGy		NaBaBSi 5 MGy		LiNaBSi 0.5 MGy		LiNaBSi 5 MGy	
g-values	**Defect**	**g-values**	**Defect**	**g-values**	**Defect**	**g-values**	**Defect**

2.018	E^- polaron/BOHC	2.016	E^- polaron/BOHC	2.019	BOHC	2.018	BOHC
2.009	BOHC	2.007	BOHC	2.011	BOHC	2.010	BOHC
2.001	BOHC	2.000	BOHC	2.004	BOHC	2.003	BOHC
1.993	ET	1.991	ET	1.997	ET	1.996	ET
1.974	E^- polaron	1.972	E^- polaron	-	-	-	-

Peak-to-peak first and second-derivative EPR absorption intensities, plotted for NaBaBSi glasses irradiated with 0.5 and 5 MGy at room temperature and annealed at 373 -773 K for 16 and 24 hours, are given in Figures S2-S9 (Supplementary information). All resonance signals due to paramagnetic radiation-induced defect centres present in the EPR spectra for NaBaBSi glass after 0.5 MGy irradiation remain after annealing at 373 K for 16 hours, as shown in Figure S3. At temperatures greater than 373 K the signals disappear upon annealing, which is attributed to defect recombination / annihilation.

In Figure S5 an underlying signal for the NaBaBSi glass irradiated with 0.5 MGy appeared after annealing at 473 K for 24 hours. This signal appears to be a combination of two paramagnetic centres. The g-value calculated from the second-derivative spectra is g~1.998 and this resonance is attributed to E' (electrons trapped on three-fold coordinated Si atoms) centres plus a nearby shoulder [22][38][39]. This signal did not appear after annealing at 473 K for 16 hours but appeared when annealed for 24 hours. This suggests that the charged particle (electron in this case) created in the glass by irradiation, after gaining thermal energy through annealing, is more mobile, migrates from its original position, and becomes trapped at a different site: a time-dependent effect. The signal at g ~1.97 ± 0.002, which is attributed to E-centres, remains stable at 473 K but disappears at higher temperatures [20][33][34].

In Figure S7, EPR shows that the defects present in the NaBaBSi glass irradiated with 5 MGy remain stable after annealing at 373 K for 16 hours. After annealing at 473 K, the signal which appeared after the recombination of BOHCs appears to be due to peroxy-radicals (PORs) or interstitial O_2^- ions (g values g ≈ 2.005, 1.999, as described in [22][38][39][47]). The POR has a molecular structure (≡Si-O-O•) and is defined as a hole trapped on a non-bridging oxygen or O_2^- bonded to one Si atom in the glass matrix; it is also known as an oxy-defect, and has been reported by several authors [22][38][43][44][45][48][49][50]. The POR is formed either by the breakage of the peroxy-linkage (≡Si-O-O-Si≡), or by the capture of O_2^- on three-fold coordinated

Si ions. This signal remains stable at 573 K and, at higher temperatures, the S/N peak-to-peak intensity becomes low, indicating low abundance and different stages of annealing, as reported by Griscom *et al.* [51] for PORs (see Figure S7).

In Figure S9, the EPR signal for the NaBaBSi glass irradiated with 5 MGy remains stable after annealing at 473 K for 24 hours and can be attributed to PORs [38][45][51]. The peak-to-peak intensities become very weak after annealing at temperatures higher than 573 K, indicating low abundance or different stages of annealing. The signal at g~1.97 ± 0.002 is attributed to E^- centres and remains stable at 473 K, disappearing at higher temperatures [22][36][37].

Peak-to-peak first and second-derivative EPR absorption intensities for the LiNaBSi glass irradiated with 0.5 and 5 MGy at room temperature and annealed at 373 - 773 K for 16 and 24 hours are given in Figures S10-S17 (Supplementary Information). In Figure S11, after annealing at 473 K a new EPR signal arises, which may be due to PORs with g ≈2.004, 1.999 (see [22][38][39][47]), along with a low signal nearby. This resonance remains after annealing at 573 K, with decreasing S/N and peak-to-peak intensity at higher temperatures again indicating a low abundance or different stages of annealing of PORs. The changed line shape resembles that for an E' centre, although with a broader linewidth than has been reported for E' centres (0.25 mT, see Fig. S10 in Supplementary Information) [22][38]. The EPR signal attributed to the PORs (g ≈ 2.017, 2.005, 2.000) shown in Figure S13 is observed at 473 K, even after annealing at 24 hours, along with a low-intensity signal at g ~1.992 attributable to ET centre. This combination of resonances remains after annealing at 573 K with decreasing S/N and peak-to-peak intensity at higher temperatures.

EPR signals remain stable for LiNaBSi glass irradiated with 5 MGy and annealed at 373 K at 16 and 24 hours, as shown in Figures S15 and S17, respectively. After annealing at 473 K the resonance that appears has a shape (see [38][45] for the shape of PORs) consistent with PORs (Figure S14 in Supplementary Information). This resonance remains stable at 573 K, with decreasing S/N and peak-to-peak intensity at higher temperatures. The change in duration of annealing has no major impact on the types of defects remaining after annealing at higher temperatures.

Figures S18-S21 (see Supplementary Information) show temperature versus log (integrated spectral area) plots for NaBaBSi and LiNaBSi glasses irradiated with 0.5

and 5 MGy and annealed at 373-773 K for 16 and 24 hours. There is a decrease in the integrated area with increasing temperature above 373 K, showing a reduction in the concentration of paramagnetic defects.

3.3. Raman Spectroscopy

Figure 3 shows Raman spectra for NaBaBSi pristine and gamma- irradiated glasses with doses of 0.5 and 5 MGy. Spectra can be divided into three main regions. Spectral features in region 1, between 200 and 850 cm^{-1}, are due to mixed stretching and bending modes of Si-O-Si vibrational units, and ring breathing modes of borate or borosilicate ring unit groups [52][53][54]. The broad band at ~ 530 cm^{-1} is attributable to bending and stretching vibration modes of Si-O-Si units [52][53][54]. The origins of the peak centred at ~ 630 cm^{-1} are debated and it may be due to vibrations involving danburite units [53][55][56]. The peak at ~ 750 cm^{-1} can be attributed to 4-coordinated diborate and boroxol ring vibrational units [13][56] [57][58]. Region 2, 850-1250 cm^{-1}, includes peaks from Q^n Si vibrational modes (where Q^n denotes a silicate tetrahedron with *n* bridging oxygens) [52][53]. The peak at ~ 940 cm^{-1} has been attributed to Q^2 (2 bridging oxygens) units and the peak at ~1050 cm^{-1} has been attributed to Q^3 (3 bridging oxygens) units [55][57][59]. Region 3, from 1200 to 1600 cm^{-1}, includes B-O vibrational units [56][57][60]. The peak at ~ 1450 cm^{-1} is attributed to B-O vibrational units [53][61]. The Raman spectra for 0.5 and 5 MGy irradiated NaBaBSi glasses appear closely similar, with no noticeable shifts in the peak positions between spectra.

Figure 3. *Raman spectra for NaBaBSi glasses: pristine and gamma irradiated with doses of 0.5 and 5MGy.*

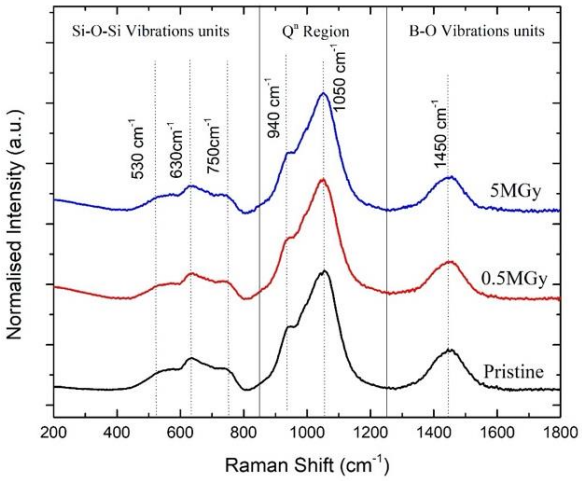

Figure 4. *Raman spectra for LiNaBSi glasses: pristine and gamma irradiated with doses of 0.5 and 5MGy.*

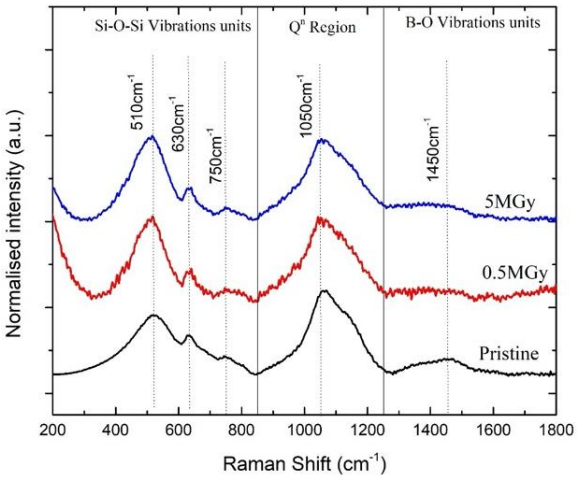

Figure 4 shows Raman spectra of pristine and gamma irradiated LiNaBSi glasses. Raman spectra were acquired between 100 and 2000 cm^{-1} and normalised using the intensity of the highest peak of the appropriate pristine glass spectrum. Similarly, to the spectra for NaBaBSi glasses, LiNaBSi glass Raman spectra were also divided into same three main regions and display similar vibrational modes. The notable differences in the Raman spectra of LiNaBSi glasses compared to NaBaBSi glasses are: (1) increased intensities of peaks in region 1; increase in the bending and stretching vibrations modes of Si-O-Si units and increase in the 4-coordinated diborate and boroxol rings suggesting network polymerisation (2) distinct shoulder at ~ 1150 cm^{-1} which can be attributed to Q^4 units [53][57]; and (3) decreased intensity of the peak at ~ 1450 cm^{-1} (decrease in three coordinated boron) [62][63].

3.4. UV-Vis nIR Optical Absorption Spectroscopy

Figures 5 and 6 show UV-Vis nIR optical absorption spectra for NaBaBSi and LiNaBSi pristine and irradiated glasses specimens, respectively. The pristine glasses are transparent in the UV-visible region. After gamma irradiation a broad band arises in the range 560-660 nm in NaBaBSi irradiated specimens and 500-640 nm in LiNaBSi irradiated specimens. Interactions of gamma photons with the glass structure cause breaking of the 3D network, leading to the transformation of BO (bridging oxygen) to NBO (non-bridging oxygen) units [64].

Figure 5. *UV-Vis-nIR optical absorption spectra for pristine, 0.5 and 5 MGy NaBaBSi glass specimens.*

Figure 6. *UV-Vis nIR optical absorption spectra for pristine, 0.5 and 5 MGy LiNaBSi glass specimens.*

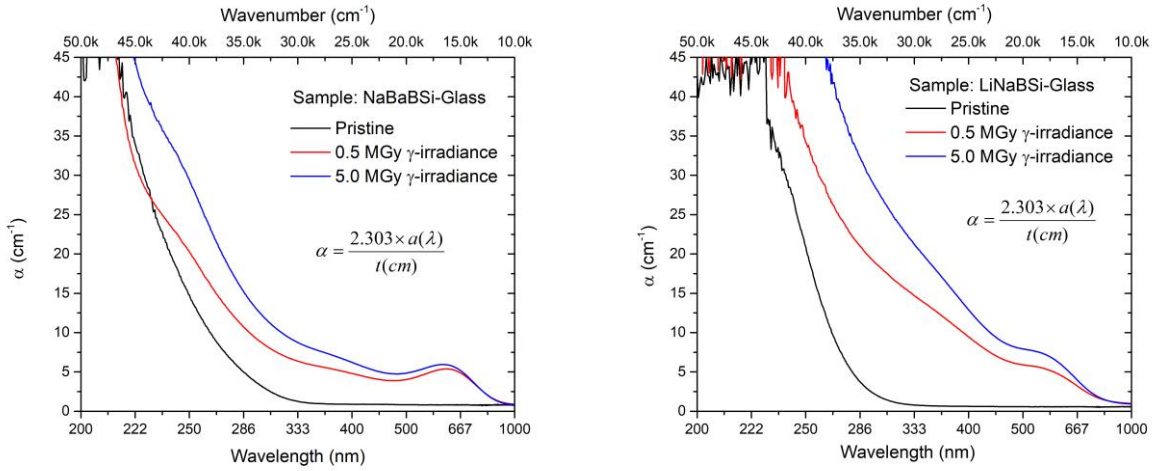

Table 4. *Band gap energies obtained from Tauc plots for optical bands observed in pristine and irradiated NaBaBSi and LiBaBSi glass specimens.*

	Band gap / eV	
Dose (MGy)	NaBaBSi	LiNaBSi
0	3.50	3.90
0.5	2.90	2.20
5	2.70	1.50

The optical band gap energies were calculated and are given in Table 4 from Tauc-Plots for 0 (pristine), irradiated with 0.5 MGy and 5 MGy NaBaBSi and LiNaBSi glass specimens. The decrease in the optical band gap energies with increasing gamma dose is attributed to the formation of non-bridging oxygens due to irradiation [64][65]. Tauc-Plots for 0 (pristine), irradiated with 0.5 MGy and 5 MGy NaBaBSi glass specimens, are provided in the Supplementary Information (Figures S22 and S23).

Figures 7 and 8 show the deconvolution of UV-Vis-nIR spectra for NaBaBSi and LiNaBSi glasses, respectively. Four Gaussian peaks were fitted to spectra for both glasses irradiated with 0.5 and 5 MGy. Fitting parameters are given in Table S9 in the Supplementary Information. For NaBaBSi glass irradiated with 5 MGy an absorption band at 657 nm and a band at 639 nm in 0.5 MGy irradiated glass can be

attributed to an overlap of E^- and PORs [66][67]. Griscom *et al.* [66] reported absorption bands due to PORs at 629 nm and non-bridging oxygen hole centers (NBOHC) at 566 nm in fused silica. Mackey *et al.* [67] reported absorption bands due to E^- centres in the range 600-730 nm in high-purity SiO_2-Na_2O glasses irradiated with X-rays. Fayad *et al.* [68] reported absorption bands between 500 and 600 nm due to BOHC's in gamma-irradiated borosilicate glasses and absorption bands at 527 and 568 nm can also be attributed BOHC's or hole trapped centres [68]. Absorption bands at 319 and 324 nm can be attributed due to trapped electrons of alkali or Na^+ ions (plasmon band) as also reported by Jiang *et al.* [69] and Mackey *et al.* [70]; and the bands at 249 and 253 nm can be attributed to Fe trace impurities [68][71][72]. For LiNaBSi glass irradiated with 0.5 MGy an absorption band at 568 nm can be attributed to a combination of BOHC and POR's and a band at 622 nm for glass irradiated with 5 MGy is attributed to BOHC [68][73]. Absorption bands at 354, 376 and 551 nm can also be attributed to BOHC or hole trapped centres [70][73]. Bands at 274 and 289 nm can be attributed to ET centres and a band at 263 nm can be attributed due to Fe impurities [68][70][71][72].

Table 5. *Summary of radiation induced optical absorption band and defects causing them.*

NaBaBSi		**LiNaBSi**	
0.5 MGy	**5 MGy**	**0.5 MGy**	**5 MGy**
639 nm (E^- centres + PORs) [66][67]	657 nm (E^- centres + PORs) [66][67]	568 nm (BOHC+ PORs) [66][68][73]	622 nm (BOHC) [73]
527 nm (BOHC)[68]	568 nm (BOHC)[68]	354 nm (BOHC)[73]	551 nm (BOHC)[68]
324 nm (E^- centre)[69]	319 nm (E^- centre)[69]	289 nm (ET centres)[70]	376 nm (BOHC) [73]
253 nm (Fe impurity)[68][71]	249 nm (Fe impurity)[68][71]	263 nm (Fe impurity)[68][71]	274 nm (ET centres) [70]

Figure 7. *Deconvolution of UV-Vis-nIR optical absorption spectra for pristine, 0.5 and 5 MGy NaBaBSi glass specimens.*

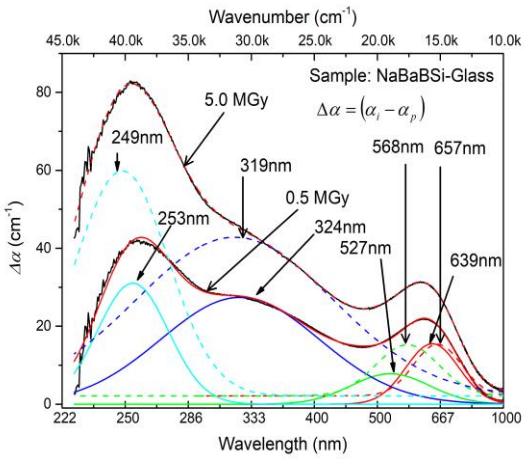

Figure 8. *Deconvolution of UV-Vis-nIR optical absorption spectra for pristine, 0.5 and 5 MGy LiNaBSi glass specimens.*

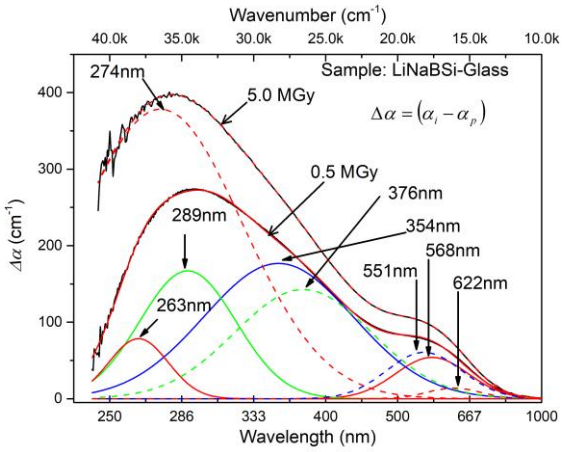

4. Discussion

4.1 Radiation-induced defects at room temperature

Radiation effects in different glasses have been studied by many researchers over the last 50 years using EPR spectroscopy [42][43][74][75][76][77][78]. EPR spectroscopy is particularly useful in studying paramagnetic radiation-induced defects in materials, and it can also elucidate information on some transition metal and lanthanide components, even at trace (impurity) levels, and provide structural information. Gamma irradiation induced changes in Indian (NaBaBSi) representative (Trombay nuclear waste) glass have been studied by Mohapatra *et al*. [38][79] while McGann *et al.* [80] studied gamma radiation effects in UK representative HLW and ILW (intermediate level waste) glasses. Only a few studies are reported in the literature for the 4-oxide Indian (NaBaBSi) and UK (LiNaBSi) base glasses before addition of HLW waste (or inactive surrogate waste).

According to Weber *et al*. [3] and Boizot *et al.* [81] alkali ions in “base” glasses can, upon irradiation, act as electron traps [82] and form colloidal metallic clusters via similar mechanisms to those observed for alkali halide crystals. Griscom [36] suggested that alkali-ions may cluster in alkali borate glasses and agglomerate to form bigger complexes after trapping of an electron, making the electron trapped

centres non-paramagnetic (spin-paired). He further suggested that such processes are thermally-activated i.e. that alkali ions with trapped electrons agglomerate, and this is one explanation here for the EPR signal we observed at room temperature arising from hole-trapped centres alone. Brow [83] reported the formation metallic sodium on the surface of irradiated binary sodium silicate glass. Howitt *et al.* [84] proposed mechanisms for the formation of metallic sodium in binary SiO_2-Na_2O glasses shown in (1-3) below, and a similar mechanism may arise in borosilicate glasses.

Si-O-Si or B-O-B (formation of NBOs by irradiation by modifier or radiation) (1)

$Si\text{-}O\cdots Na^+ + hv \rightarrow Si\text{-}O: + Na^+$ (breaking of ionic or electrostatic bond) (2)

$Si\text{-}O: + Na^+ + hv \rightarrow Si\text{-}O\cdot + Na$ (creation of oxide radical and metallic Na) (3)

Hassib *et al.* [85] found an EPR signal at g = 2.011 due to sodium colloids formed by the collapse of F-centres in sodalite ($Na_8(Al_6Si_6O_{24})Cl_2$). Zatsepin *et al.* [37] reported the presence of E^- centres at g = 1.97 at higher magnetic fields (~345-350 mT) in Na/K silicate glasses.

In addition to EPR, optical absorption spectroscopy has also long been used to elucidate radiation-induced defects or “colour centres”. Electrons and holes trapped at defect sites within the glass structure give optical absorption bands in UV, visible, and near infrared region [86]. The presence of atomically dispersed metallic sodium colloids in different materials can be confirmed by the plasmon absorption band and by the color (typically blue) which they induce to the material and this is reported by many researchers (Table S10). The plasmon absorption band can be located at different wavelengths depending on the size and shape of the colloidal particle [87][88]. Groote *et al.* [89][86][90][91] reported a broad optical absorption band centred at 550-600 nm for an electron irradiated NaCl crystal and, based on this and differential scanning calorimetry (DSC) results, suggested that the metallic colloid particles present were of different sizes and shapes and show different melting behaviours (sodium colloids in different shape and size of melt at different temperatures). Wesełucha-Birczyńska *et al.* [92] reported a plasmon band at 629 nm for navy blue single crystals for natural halite and at 621 nm for blue samples. Tsai *et al.* [93] found an EPR signal at g~2.01 and an absorption band in the range 360-540

nm for gamma irradiated silicate glasses. Jiang *et al.* [94] found a plasmon band using electron energy loss spectroscopy (EELS) in electron irradiated sodium silicate glass. Bochkareva *et al.* [88] reported a plasmon resonance absorption band at 405-410 nm in Na containing silicate glasses. Mackey *et al.* [67][70] also reported a resonance plasmon absorption band due to Na nanoparticles in silicate glasses. The list in Table S10 is not exhaustive but presents significant supporting evidence for formation of metallic colloids in irradiated alkali-halide and glass systems, identified using mainly EPR and optical absorption spectroscopies. While both NaBaBSi and LiNaBSi glass specimens studied here, irradiated with 0.5 and 5 MGy, show formation of BOHCs and ET centres, a broad isotropic signal at g~2.011 and ~1.97 is tentatively attributed to metallic sodium colloids (nanoparticles) in the NaBaBSi glass alone. The difference (increase with dose) in the intensity of the resonance peaks suggests that the concentration of defects may be different at different doses.

4.2 Effects of glass composition and structure

The relation between physical properties of a glass and composition is non-linear when the relative proportion of alkalis is changed in a mixed alkali glass [97][98]. This is called mixed-alkali effect. This may have impacts on glass modifier mixing (homogenous or clustering), cation diffusivities and nucleation of crystals [29]. The lower concentration of Na in the LiNaBSi glass compared to NaBaBSi glass (concentration of Na is almost double in NaBaBSi glass), the high cationic field strength of Li^+ and greater association with NBOs than Na^+, as reported by Mishra *et al.* [30] Kaushik *et al.* [31] and Mishra *et al.* [32], and the heterogeneity and nanoscale immiscibility (due to the mixed-alkali effect) do not favour the clustering of defects or alkali ions. In the NaBaBSi glass Na^+ ions are associated with NBOs due to its high concentration and its smaller ionic radius than Ba^{2+}, which favour the segregation and formation of metallic sodium colloids via electron capture [27][29][30][31]. The observations are further supported by the presence of a broad UV-Vis IR absorption band in the range 560-660 nm, indicative of different sizes of metallic sodium colloids causing the blue colour of the glass. The position of the band depends on the environment around the Na nanoparticles and hence different authors have reported different positions for plasmon resonance absorption band for different materials. Kordas *et al.* [75] reported that it is difficult to detect metallic sodium using EPR as these ionic electron trapping centres cannot be observed at

room temperature because of the short spin-grid relaxation time. Griscom *et al.* [42] suggested that at temperatures ≤ 77 K electrons are trapped at alkali and alkali clusters in sodium and potassium borate glasses. However, we have found these EPR signals at room temperature and this might be attributable to resonant absorption of microwaves by conduction electrons within sodium metallic particles of small size.

4.3 Effects of thermal annealing on radiation-induced defects

In Figures S3 and S5, EPR signals disappeared after annealing at temperatures higher than 473 K for NaBaBSi glass specimens irradiated with 0.5 MGy and annealed at 16 and 24 hours, respectively, suggesting that thermal energy enables electron-hole pair recombination; and there is no paramagnetic defect generated at the lower dose of 0.5 MGy which is stable at higher temperatures [78]. The signal due to E^- centres at g~1.97 remains stable after annealing at 473 K but the broad, isotropic signal at g~2.011 disappeared after annealing at 373 K. Both resonances may be due to metallic sodium colloids. Since sodium colloids of different size and shape melt at different temperatures [89], this suggests that there may be two differently-sized distributions of metallic sodium colloids present in the glass.

The appearance of a combination of signals due to E' and ET centres after annealing suggests that thermal energy can enable a charged particle to occupy different sites in the glass structure. At the higher dose of 5 MGy, an underlying signal appeared when the samples were annealed at 473 K for 16 hours as well as 24 hours. This signal has been attributed to PORs [38][50]. The signal remains stable at 573 K and at higher temperatures the S/N peak-to-peak intensity decreases, suggesting low abundance or different stages of annealing. PORs can form in the glass structure via the breakage of peroxy- linkage by a gamma photon [99], as shown in (4).

$$\text{Si-O-O-Si} + h\nu \rightarrow \text{Si-O-O}\cdot + \cdot\,\text{Si} \quad (4)$$

A POR can further form an E' (Si·) centre and molecular oxygen as shown in (5).

$$\text{Si-O-O}\cdot + h\nu \rightarrow \text{Si}\cdot + O_2 \quad (5)$$

The possible change of PORs into E' and molecular oxygen at higher temperature suggests that thermal energy can also remove PORs [100][101]. For LiNaBSi glass

specimens irradiated with low dose (0.5 MGy) the EPR signals revealed after annealing at 473 K are due to PORs and a decrease in the S/N peak-to-peak intensity at higher temperatures [38][50]. The same effects are seen at the higher dose; however, S/N peak-to-peak intensity is higher, indicating an increased concentration of number of defects with increased dose. Figures S18-S21 show a clear decrease of the number of defects, as shown by the decrease in log (area) of the integral of the first derivative absorption with increasing temperature.

Wasteform canister centreline cooling (CCC) temperature will vary as a function of time and dimensions and depend on the radionuclides / activity as well as thermal history of the waste [102]. CCC temperatures can range from 370 K – 570 K and can be as high as 670 K [13][103]. Gamma-induced defects such as PORs, which can be the precursors for molecular oxygen and E' centres in both of the studied glasses, are stable at CCC temperatures, and this result may thus be of relevance to geological disposal in future technical assessments that go beyond the current generic scenario for geological disposal [104]. These microstructural changes relax with time and temperature, as demonstrated here by their decreasing intensities. However, there are permanent changes associated with them, in addition to cumulative effects of beta and alpha decay, which may have major impacts on structural integrity of the waste form. The glass structure becomes free from any decoupled modes (vibrating modes decoupled from the glass forming network) much below the glass transition, however, some modes remain active during cooling and continue to be active in the glassy state [1]. Near the glass transition temperature (T_g) the glass network stabilizes, the mobility (migration and annihilation) of the defects is reduced and thus radiation defects can persist, as shown by this study.

Boizot *et al.* [105] studied three simple glass compositions under beta irradiation using Raman spectroscopy. They reported an increased in silicate network polymerisation due to relative increase of the Q^3/Q^2 species concentration, an increase in concentration of molecular oxygen O_2 and decrease in the average Si-O-Si bond angle under beta irradiation relative to pristine samples. They attributed this structural evolution to the migration and aggregation of sodium ions. Similar structural evolution was observed by Abbas *et al.* [106] in their study of two simple glasses studied under alpha, and Kr-ion irradiations. In the present study there are no substantial structural changes or any new bands that could be attributed to the

formation of molecular oxygen; and no large changes in the boron region observed using Raman spectroscopy. A further investigation of Q^n units (n is number of bridging oxygens in Si tetrahedron) using other techniques such as ^{29}Si and ^{11}B MAS-NMR could provide more information on the glass network after irradiation. Nanoscale structural probing using TEM or another technique to inspect bulk-irradiated samples for both the glasses would be useful to develop further understanding of the characteristics of metallic sodium colloids, and ^{23}Na MAS-NMR may therefore also prove beneficial.

4.4 Effects of multivalent elements on radiation-induced defects

HLW comprises of many multivalent elements. The oxidation-reduction chemistry of these elements is very complex [107]. During melting and in the vitrified glass product the behaviour of these multivalent cations depends on the stable oxidation state. While some of these for e.g. Mo, Ru, S etc. can be problematic in terms of their solubility, processing, leachability, foaming and so on, many could be advantageous in mitigating the radiation induced paramagnetic defects [107]. Several studies have shown that multivalent cations like rare earths (Yb, Gd, Eu) and transition metals (Fe, Mn, Cr) mitigate radiation-induced defect generation and structural changes by the trapping of free electrons and holes [38][80][108][109][110][111]. This defect-hopping or electron/holes trapping process is expected in NaBaBSi and LiNaBSi glasses when doped with actual waste components under optimum redox conditions. The formation of radiation-induced Na colloids may also be hindered in NaBaBSi glass doped with actual HLW waste components; however, it would be interesting to study Indian HLW waste which is higher in Na concentration [112].

5. Conclusions

The effects of gamma irradiation on NaBaBSi and LiNaBSi glasses were investigated. Both glass specimens were irradiated with 0.5 and 5 MGy of gamma radiation. The objective of this study was to improve understanding of the types of radiation-induced defects and establish a study of their thermal stability at geological repository relevant temperatures and how/whether these are affected by glass composition. Room temperature X-band EPR spectroscopy was employed to investigate gamma irradiation-induced defects along with UV-Vis-nIR optical

absorption and Raman spectroscopies. The paramagnetic defect centres identified for NaBaBSi glass at both the doses are BOHC, E^- centres (g~1.97) and isotropic signal at g~2.011 both due to the colloidal metallic sodium particles. UV-Vis-nIR results for NaBaBSi glass showed absorption bands due to E^- centres at 639 and 657 nm, which confirms the presence of metallic sodium colloids and the associated blue colour post-irradiation, supported by evidence from the literature. UV-Vis-nIR also showed absorption bands due to PORs, BOHC and electron trapped centres. In LiNaBSi glass BOHC, ET centres are identified at both the doses. Thermal annealing at temperatures above 473 K for 0.5 MGy irradiated NaBaBSi glass enables the annihilation / recombination of the defects, whereas in the LiNaBSi glass, PORs are stable at 473 K and show decreasing S/N peak-to-peak intensity with increasing temperature. PORs or O_2^- interstitials are stable in the LiNaBSi glass irradiated with 5 MGy at temperatures higher than 573 K, whereas the NaBaBSi glass irradiated with 5 MGy showed comparatively low S/N peak-to-peak intensity at higher temperatures. Moreover, it can be expected that increasing the duration of the thermal annealing can remove / bleach the defects, however, there are permanent microstructural changes which can have significant impact on the durability of the waste form. The presence of sodium metallic colloids of differing sizes is a strong indication of radiation-induced formation of nanoparticles, which should be further investigated as these may form macroscopic clusters depending on glass composition, any temperature gradient, or locally-induced electric fields.

Acknowledgements

The authors acknowledge the support of The University of Manchester's Dalton Cumbrian Facility (DCF), a partner in the National Nuclear User Facility, the EPSRC UK National Ion Beam Centre and the Henry Royce Institute. We also thank the Ministry of Social Justice and Empowerment, the Government of India for providing the funds for this Ph.D. research. We also thank Dr. Shuchi Vaishnav, Prof. Georges Calas and Dr. Laurence Galoisy for useful discussions.

References

[1] R.C. Ewing, W.J. Weber, F.W. Clinard, Radiation effects in nuclear waste forms for high-level radioactive waste, Prog. Nucl. Energy. 29 (1995) 63–127. https://doi.org/10.1016/0149-1970(94)00016-Y.

[2] M.T. Harrison, Vitrification of high level waste in the UK, Procedia Mater. Sci. 7 (2014) 10–15. https://doi.org/10.1016/j.mspro.2014.10.003.

[3] W.J. Weber, R.C. Ewing, C.A. Angell, G.W. Arnold, A.N. Cormack, J.M. Delaye, D.L. Griscom, L.W. Hobbs, A. Navrotsky, D.L. Price, A.M. Stoneham, M.C. Weinberg, Radiation Effects in Glasses Used for Immobilization of High-level Waste and Plutonium Disposition, J. Mater. Res. 12 (1997) 1948–1978. https://doi.org/10.1557/jmr.1997.0266.

[4] C.M. Jantzen, Systems approach to nuclear waste glass development, J. Non. Cryst. Solids. 84 (1986) 215–225. https://doi.org/10.1016/0022-3093(86)90780-5.

[5] N.J. Cassingham, P. Bingham, R.J. Hand, S. Forder, Property modification of a high level nuclear waste borosilicate glass through the addition of Fe_2O_3, Glas. Technol. Eur. J. Glas. Sci. Technol. A, Febr. 2008, 49 (1), 21–26. 49 (2008) 21–26. http://www.societyofglasstechnology.org.uk/cgi-bin/open.cgi?page=journal&sessionid=85597106.

[6] I.W. Donald, B.L. Metcalfe, R.N.J. Taylor, Review The immobilization of high level radioactive wastes using ceramics and glasses, J. Mater. Sci. (1997) 5851–5887.

[7] W.J. Weber, F.P. Roberts, A review of radiation effects in solid nuclear waste forms, Nucl. Technol. 60 (1983) 178–198. https://doi.org/10.13182/NT83-A33073.

[8] W.J. Weber, A. Navrotsky, S. Stefanovsky, E.R. Vance, E. Vernaz, Materials Science of High-Level Immobilization, MRS Bull. 34 (2009) 46–52. https://doi.org/10.1557/mrs2009.12.

[9] W.J. Weber, L.R. Corrales, N.J. Ness, R.E. Williford, H.L. Heinisch, S. Thevuthasan, J.P. Icenhower, B.P. McGrail, R. Devanathan, R.M. VanGinhoven, J. Song, B. Park, W. Jiang, B.D. Begg, R.B. Birtcher, X. Chen, S.D. Conradson, Radiation Effects in Nuclear Waste Materials October 2000 Prepared for the U . S . Department of Energy, PNNL-13345. (2000).

[10] S. Gin, A. Abdelouas, L.J. Criscenti, W.L. Ebert, K. Ferrand, T. Geisler, M.T. Harrison, Y. Inagaki, S. Mitsui, K.T. Mueller, J.C. Marra, C.G. Pantano, E.M. Pierce, J. V. Ryan, J.M. Schofield, C.I. Steefel, J.D. Vienna, An international initiative on long-term behavior of high-level nuclear waste glass, Mater. Today. 16 (2013) 243–248. https://doi.org/10.1016/j.mattod.2013.06.008.

[11] C.S. N.Jacquet-Francillon, R. Bonniaud, Glass as a Material for the Final Disposal of Fission Products, Radiochim. Acta. 240 (1979) 231–240.

[12] W.G. Burns, A.E. Hughes, J.A.C. Marples, R.S. Nelson, A.M. Stoneham, Effects of radiation on the leach rates of vitrified radioactive waste, J. Nucl. Mater. 107 (1982) 245–270. https://doi.org/10.1016/0022-3115(82)90424-X.

[13] A.H. Mir, I. Monnet, B. Boizot, C. Jégou, S. Peuget, Electron and electron-ion sequential irradiation of borosilicate glasses: Impact of the pre-existing defects, J. Nucl. Mater. 489 (2017) 91–98. https://doi.org/10.1016/j.jnucmat.2017.03.047.

[14] W.J. Weber, Radiation and Thermal Ageing of Nuclear Waste Glass, Procedia Mater. Sci. 7 (2014) 237–246. https://doi.org/10.1016/j.mspro.2014.10.031.

[15] S. Gin, P. Jollivet, M. Tribet, S. Peuget, S. Schuller, Radionuclides containment in nuclear glasses: An overview, Radiochim. Acta. 105 (2017) 927–959. https://doi.org/10.1515/ract-2016-2658.

[16] B. Boizot, G. Petite, D. Ghaleb, G. Calas, Dose, dose rate and irradiation temperature effects in β-irradiated simplified nuclear waste glasses by EPR spectroscopy, J. Non. Cryst. Solids. 283 (2001) 179–185. https://doi.org/10.1016/S0022-3093(01)00338-6.

[17] K.B. Patel, B. Boizot, S.P. Facq, S. Peuget, S. Schuller, I. Farnan, Impacts of composition and beta irradiation on phase separation in multiphase amorphous calcium borosilicates, J. Non. Cryst. Solids. 473 (2017) 1–16. https://doi.org/10.1016/j.jnoncrysol.2017.06.018.

[18] P.A. Bingham, G. Yang, R.J. Hand, G. Möbus, Boron environments and irradiation stability of iron borophosphate glasses analysed by EELS, Solid State Sci. 10 (2008) 1194–1199. https://doi.org/10.1016/j.solidstatesciences.2007.11.024.

[19] N. Jiang, J. Silcox, High-energy electron irradiation and B coordination in Na_2O-B_2O_3-SiO_2 glass, J. Non. Cryst. Solids. 342 (2004) 12–17. https://doi.org/10.1016/j.jnoncrysol.2004.07.001.

[20] B. Boizot, N. Ollier, F. Olivier, G. Petite, D. Ghaleb, E. Malchukova, Irradiation effects in simplified nuclear waste glasses, Nucl. Instruments Methods Phys. Res. Sect. B Beam Interact. with Mater. Atoms. 240 (2005) 146–151. https://doi.org/10.1016/j.nimb.2005.06.105.

[21] N. Jiang, J. Silcox, Electron irradiation induced phase decomposition in alkaline earth multi-component oxide glass, J. Appl. Phys. 92 (2002) 2310–2316. https://doi.org/10.1063/1.1496148.

[22] B. Boizot, G. Petite, D. Ghaleb, G. Calas, Radiation induced paramagnetic centers in nuclear glasses by EPR spectroscopy, Nucl. Inst. Methods Phys. Res. B. 141 (1998) 580–584.

[23] C. Huang, A.N. Cormack, Structural differences and phase separation in alkali silicate glasses, J. Chem. Phys. 95 (1991) 3634–3642. https://doi.org/10.1063/1.460814.

[24] Y.H. Yun, P.J. Bray, Nuclear magnetic resonance studies of the glasses in the system Na_20-B_20_3-SiO 2, J. Non. Cryst. Solids. 30 (1978) 45–60. https://doi.org/10.1016/0022-3093(78)90055-8.

[25] W.J. Dell, P.J. Bray, S.Z. Xiao, 11B NMR studies and structural modeling of Na_2O-B_2O_3-SiO_2 glasses of high soda content, J. Non. Cryst. Solids. 58 (1983) 1–16. https://doi.org/10.1016/0022-3093(83)90097-2.

[26] P. Zhao, S. Kroeker, J.F. Stebbins, Non-bridging oxygen sites in barium borosilicate glasses: Results from 11B and 17O NMR, J. Non. Cryst. Solids. 276 (2000) 122–131. https://doi.org/10.1016/S0022-3093(00)00290-8.

[27] L.S. Du, J.F. Stebbins, Solid-state NMR study of metastable immiscibility in

alkali borosilicate glasses, J. Non. Cryst. Solids. 315 (2003) 239–255. https://doi.org/10.1016/S0022-3093(02)01604-6.

[28] J.W. MacKenzie, A. Bhatnagar, D. Bain, S. Bhowmik, C. Parameswar, K. Budhwani, S.A. Feller, M.L. Royle, S.W. Martin, 29Si MAS-NMR study of the short range order in alkali borosilicate glasses, J. Non. Cryst. Solids. 177 (1994) 269–276. https://doi.org/10.1016/0022-3093(94)90540-1.

[29] L.S. Du, J.F. Stebbins, Site preference and Si/B mixing in mixed-alkali borosilicate glasses: A high-resolution ^{11}B and ^{17}O NMR study, Chem. Mater. 15 (2003) 3913–3921. https://doi.org/10.1021/cm034427r.

[30] R.K. Mishra, S. Kumar, B.S. Tomar, A.K. Tyagi, C.P. Kaushik, K. Raj, V.K. Manchanda, Effect of barium on diffusion of sodium in borosilicate glass, J. Hazard. Mater. 156 (2008) 129–134. https://doi.org/10.1016/j.jhazmat.2007.12.006.

[31] C.P. Kaushik, R.K. Mishra, P. Sengupta, A. Kumar, D. Das, G.B. Kale, K. Raj, Barium borosilicate glass – a potential matrix for immobilization of sulfate bearing high-level radioactive liquid waste, J. Nucl. Mater. 358 (2006) 129–138. https://doi.org/10.1016/j.jnucmat.2006.07.004.

[32] R.K. Mishra, V. Sudarsan, C.P. Kaushik, K. Raj, S.K. Kulshreshtha, A.K. Tyagi, Effect of BaO addition on the structural aspects and thermophysical properties of sodium borosilicate glasses, J. Non. Cryst. Solids. 353 (2007) 1612–1617. https://doi.org/10.1016/j.jnoncrysol.2007.01.074.

[33] R.K. Mishra, K. V. Sudarsan, P. Sengupta, R.K. Vatsa, A.K. Tyagi, C.P. Kaushik, D. Das, K. Raj, Role of sulfate in structural modifications of sodium barium borosilicate glasses developed for nuclear waste immobilization, J. Am. Ceram. Soc. 91 (2008) 3903–3907. https://doi.org/10.1111/j.1551-2916.2008.02773.x.

[34] L. Leay, W. Bower, G. Horne, P. Wady, A. Baidak, M. Pottinger, M. Nancekievill, A.D. Smith, S. Watson, P.R. Green, B. Lennox, J.A. Laverne, S.M. Pimblott, Development of irradiation capabilities to address the challenges of the nuclear industry, Nucl. Instruments Methods Phys. Res. Sect. B Beam Interact. with Mater. Atoms. 343 (2015) 62–69. https://doi.org/10.1016/j.nimb.2014.11.028.

[35] D.A. Long, Raman Spectroscopy, McGraw-Hill, New York, 1977.

[36] D.L. Griscom, Alkali- Associate Trapped-Electron centers in Alkali borate glasses irradiated at 77 K, J. Non. Cryst. Solids. 6 (1971) 275–282.

[37] A.F. Zatsepin, V.B. Guseva, V.A. Vazhenin, M.Y. Artoymov, Paramagnetic defects in gamma-irradiated Na/K-silicate glasses, Phys. Solid State. 54 (2012) 1776–1784. https://doi.org/10.1134/S1063783412090326.

[38] M. Mohapatra, R.M. Kadam, R.K. Mishra, C.P. Kaushik, B.S. Tomar, S. V. Godbole, Gamma Radiation-Induced Changes in Trombay Nuclear Waste Glass Containing Iron, Int. J. Appl. Glas. Sci. 4 (2013) 53–60. https://doi.org/10.1111/j.2041-1294.2012.00094.x.

[39] M. Mohapatra, R.M. Kadam, R.K. Mishra, D. Dutta, P.K. Pujari, C.P. Kaushik,

R.J. Kshirsagar, B.S. Tomar, S. V Godbole, Electron beam irradiation effects in Trombay nuclear waste glass, Nucl. Inst. Methods Phys. Res. B. 269 (2011) 2057–2062. https://doi.org/10.1016/j.nimb.2011.06.009.

[40] D. Forum, M. Mohapatra, B. Atomic, T. Bhabha, P. View, Spectroscopic Investigations of Radiation Damage in Glasses Used for Immobilization of Radioactive Waste, (2013). https://doi.org/10.4028/www.scientific.net/DDF.341.107.

[41] M. Mohapatra, R.K. Mishra, C.P. Kaushik, B.S. Tomar, Investigation of Radiation Damage in Trombay Nuclear Waste Glasses by ESR and Photoluminescence Techniques, Procedia Mater. Sci. 7 (2014) 247–251. https://doi.org/10.1016/j.mspro.2014.10.032.

[42] D.L. Griscom, E.S.R. studies of radiation damage and structure in oxide glasses not containing transition group ions: A contemporary overview with illustrations from the alkali borate system, J. Non. Cryst. Solids. 13 (1974) 251–285. https://doi.org/10.1016/0022-3093(74)90095-7.

[43] E.J. Friebele, D.L. Griscom, M. Stapelbroek, R.A. Weeks, Fundamental defect centers in glass: The peroxy radical in irradiated, high-purity, fused silica, Phys. Rev. Lett. 42 (1979) 1346–1349. https://doi.org/10.1103/PhysRevLett.42.1346.

[44] H. Hosono, Y. Abe, Photosensitivity and structural defects in dopant-free ultraviolet-sensitive calcium aluminate glasses, J. Non. Cryst. Solids. 95–96 (1987) 717–724. https://doi.org/10.1016/S0022-3093(87)80673-7.

[45] M. Mohapatra, R.M. Kadam, R.K. Mishra, D. Dutta, P.K. Pujari, C.P. Kaushik, R.J. Kshirsagar, B.S. Tomar, S. V. Godbole, Electron beam irradiation effects in Trombay nuclear waste glass, Nucl. Instruments Methods Phys. Res. Sect. B Beam Interact. with Mater. Atoms. (2011). https://doi.org/10.1016/j.nimb.2011.06.009.

[46] H. Annersten, A. Hassib, Blue sodalite, Can. Mineral. 17 (1979) 39–46. http://canmin.geoscienceworld.org/content/17/1/39.extract.

[47] T.T. Wang, X.Y. Zhang, M.L. Sun, X. Du, M. Guan, H.B. Peng, T.S. Wang, γ-Irradiation effects in borosilicate glass studied by EPR and UV–Vis spectroscopies, Nucl. Instruments Methods Phys. Res. Sect. B Beam Interact. with Mater. Atoms. 464 (2020) 106–110. https://doi.org/10.1016/j.nimb.2019.12.007.

[48] D.L. Griscom, From E′ centers to the “characteristic” resonance: a colleague’s reminiscences on the scientific odyssey of Robert A. Weeks, J. Non. Cryst. Solids. (1994). https://doi.org/10.1016/0022-3093(94)90682-3.

[49] D.A. Dutt, P.L. Higby, D.L. Griscom, An electron spin resonance study of X-irradiated calcium aluminosilicate glasses, J. Non. Cryst. Solids. 130 (1991) 41–51. https://doi.org/10.1016/0022-3093(91)90154-X.

[50] D.L. Griscom, C.I. Merzbacher, R.A. Weeks, R.A. Zuhr, Electron spin resonance studies of defect centers induced in a high-level nuclear waste glass simulant by gamma-irradiation and ion-implantation, J. Non. Cryst. Solids. 258 (1999) 34–47. https://doi.org/10.1016/S0022-3093(99)00557-8.

[51] D.L. Griscom, C.I. Merzbacher, R.A. Weeks, R.A. Zuhr, Electron spin resonance studies of defect centers induced in a high-level nuclear waste glass simulant by gamma-irradiation and ion-implantation, J. Non. Cryst. Solids. (1999). https://doi.org/10.1016/S0022-3093(99)00557-8.

[52] Paul McMillan, Structural studies of silicate glasses and melts-applications and limitations of Raman spectroscopy, Am. Mineral. 69 (1984) 622–644. https://doi.org/10.1007/BF00307725.

[53] D. Manara, A. Grandjean, D.R. Neuville, Advances in understanding the structure of borosilicate glasses: A raman spectroscopy study, Am. Mineral. 94 (2009) 777–784. https://doi.org/10.2138/am.2009.3027.

[54] S.K.S. and J.A.P. Dean W. Matson, The structure of high-silica alkali-slicate glasses. A Raman spectroscopic investigation, J. Non. Cryst. Solids. 58 (1983) 323–352. https://doi.org/10.1093/jicru_os19.1.1.

[55] B.G. Parkinson, D. Holland, M.E. Smith, C. Larson, J. Doerr, Quantitative measurement of Q^3 species in silicate and borosilicate glasses using Raman spectroscopy, J. Non. Cryst. Solids. 354 (2008) 1936–1942. https://doi.org/10.1016/j.jnoncrysol.2007.06.105.

[56] G.F. Zhang, T.S. Wang, K.J. Yang, L. Chen, L.M. Zhang, H.B. Peng, W. Yuan, F. Tian, Raman spectra and nano-indentation of Ar-irradiated borosilicate glass, Nucl. Instruments Methods Phys. Res. Sect. B Beam Interact. with Mater. Atoms. 316 (2013) 218–221. https://doi.org/10.1016/j.nimb.2013.09.020.

[57] J. de Bonfils, S. Peuget, G. Panczer, D. de Ligny, S. Henry, P.Y. Noël, A. Chenet, B. Champagnon, Effect of chemical composition on borosilicate glass behavior under irradiation, J. Non. Cryst. Solids. 356 (2010) 388–393. https://doi.org/10.1016/j.jnoncrysol.2009.11.030.

[58] G. Karakurt, A. Abdelouas, J.P. Guin, M. Nivard, T. Sauvage, M. Paris, J.F. Bardeau, Understanding of the mechanical and structural changes induced by alpha particles and heavy ions in the French simulated nuclear waste glass, J. Nucl. Mater. 475 (2016) 243–254. https://doi.org/10.1016/j.jnucmat.2016.04.022.

[59] H. Zhang, C.L. Corkhill, P.G. Heath, R.J. Hand, M.C. Stennett, N.C. Hyatt, Effect of Zn- and Ca-oxides on the structure and chemical durability of simulant alkali borosilicate glasses for immobilisation of UK high level wastes, J. Nucl. Mater. 462 (2015) 321–328. https://doi.org/10.1016/j.jnucmat.2015.04.016.

[60] D. Manara, A. Grandjean, D.R. Neuville, Structure of borosilicate glasses and melts: A revision of the Yun, Bray and Dell model, J. Non. Cryst. Solids. 355 (2009) 2528–2531. https://doi.org/10.1016/j.jnoncrysol.2009.08.033.

[61] D.R. Neuville, L. Cormier, B. Boizot, A.M. Flank, Structure of β-irradiated glasses studied by X-ray absorption and Raman spectroscopies, J. Non. Cryst. Solids. 323 (2003) 207–213. https://doi.org/10.1016/S0022-3093(03)00308-9.

[62] F.Y. Olivier, B. Boizot, D. Ghaleb, G. Petite, Raman and EPR studies of β-irradiated oxide glasses: The effect of iron concentration, J. Non. Cryst. Solids.

351 (2005) 1061–1066. https://doi.org/10.1016/j.jnoncrysol.2005.01.018.

[63] J. Ramkumar, S. Chandramouleeswaran, V. Sudarsan, R.K. Mishra, C.P. Kaushik, K. Raj, A.K. Tyagi, Barium borosilicate glass as a matrix for the uptake of dyes, J. Hazard. Mater. 172 (2009) 457–464. https://doi.org/10.1016/j.jhazmat.2009.07.028.

[64] R. Kaur, S. Singh, O.P. Pandey, Gamma ray irradiation effects on the optical properties of BaO-Na_2O-B_2O_3-SiO_2 glasses, J. Mol. Struct. 1048 (2013) 78–82. https://doi.org/10.1016/j.molstruc.2013.05.037.

[65] J. Du, J. Wu, L. Zhao, L. Song, Color centers of a borosilicate glass induced by 10 MeV proton, 1.85 MeV electron and ^{60}Co-γ ray, Radiat. Phys. Chem. 86 (2013) 59–63. https://doi.org/10.1016/j.radphyschem.2013.01.044.

[66] D.L. Griscom, M. Mizuguchi, Determination of the visible range optical absorption spectrum of peroxy radicals in gamma-irradiated fused silica, J. Alloys Compd. 239 (1998) 66–77. https://doi.org/10.1016/s0022-3093(98)00721-2.

[67] J.H. Mackey, H.L. Smith, A. Halperin, Optical Studies in X-Irradiated High Purity Sodium Silicate Glasses, J. Phys. Chem. Solids. 27 (1966) 1759–1772.

[68] A.M. Fayad, W.M. Abd-Allah, F.A. Moustafa, Effect of Gamma Irradiation on Structural and Optical Investigations of Borosilicate Glass Doped Yttrium Oxide, Silicon. 10 (2018) 799–809. https://doi.org/10.1007/s12633-016-9533-6.

[69] N. Jiang, B. Wu, J. Qiu, J.C.H. Spence, Precipitation of nanocrystals in glasses by electron irradiation: An alternative path to form glass ceramics?, Appl. Phys. Lett. 90 (2007) 15–18. https://doi.org/10.1063/1.2724898.

[70] J.H. Mackey, H.L. Smith, J. Nahum, Competitive trapping in sodium disilicate glasses doped with Eu^{+3}, J. Phys. Chem. Solids. 27 (1966) 1773–1782. https://doi.org/10.1016/0022-3697(66)90108-9.

[71] N.A. El-Alaily, E.M.A. Hussein, F.M. Ezz Eldin, Gamma Irradiation and Heat Treatment Effects on Barium Borosilicate Glasses Doped Titanium Oxide, J. Inorg. Organomet. Polym. Mater. 28 (2018) 2662–2676. https://doi.org/10.1007/s10904-018-0934-4.

[72] T.T. Volotinen, J.M. Parker, P.A. Bingham, Concentrations and site partitioning of Fe^{2+} and Fe^{3+} ions in a soda-lime-silica glass obtained by optical absorbance spectroscopy, Phys. Chem. Glas. Eur. J. Glas. Sci. Technol. Part B. 49 (2008) 258–270.

[73] Adli Bishay, Radiation Induced Color Centers in Multicomponent Glasses, J. Non. Cryst. Solids. 3 (1970) 54–114.

[74] D.L. Griscom, Electron spin resonance in glasses, J. Non. Cryst. Solids. 40 (1980) 211–272.

[75] G. Kordas, B. Camara, H.J. OEL, Electron spin resonance studies of radiation damage in silicate glasses, J. Non. Cryst. Solids. 50 (1982) 79–95.

[76] Y. Inagaki, H. Furuya, T. Kikuchi, K. Idemitsu, Electron spin resonance studies of gamma-irradiation damage in simulatInagaki, Y., Furuya, H., Kikuchi, T., &

Idemitsu, K. (1991). Electron spin resonance studies of gamma-irradiation damage in simulated nuclear waste glass. Journal of Nuclear Science and, J. Nucl. Sci. Technol. 28 (1991) 314–320. https://doi.org/10.1080/18811248.1991.9731361.

[77] N.A. Eissa, N.H. Sheta, W.M. El-Meliga, S.M. El-Minyawi, H.A. Sallam, Mossbauer effect study of the effect of gamma irradiation on the behaviour of iron in sodium silicate glasses, Radiat Phys. Chem. 44 (1994) 35–38.

[78] L.D. Bogomolova, A.A. Deshkovskaya, N.A. Krasil'nikova, G. Battaglin, F. Caccavale, EPR study of structural defects in ion-implanted multicomponent silicate glasses, J. Non. Cryst. Solids. 151 (1992) 23–31. https://doi.org/10.1016/0022-3093(92)90005-5.

[79] M. Mohapatra, B.S. Tomar, Spectroscopic investigations of radiation damage in glasses used for immobilization of radioactive waste, Defect Diffus. Forum. 341 (2013) 107–128. https://doi.org/10.4028/www.scientific.net/DDF.341.107.

[80] O.J. McGann, P.A. Bingham, R.J. Hand, A.S. Gandy, M. Kavčič, M. Žitnik, K. Bučar, R. Edge, N.C. Hyatt, The effects of γ-radiation on model vitreous wasteforms intended for the disposal of intermediate and high level radioactive wastes in the United Kingdom, J. Nucl. Mater. 429 (2012) 353–367. https://doi.org/10.1016/j.jnucmat.2012.04.007.

[81] B. Boizot, G. Petite, D. Ghaleb, N. Pellerin, F. Fayon, B. Reynard, G. Calas, Migration and segregation of sodium under β-irradiation in nuclear glasses, Nucl. Instruments Methods Phys. Res. Sect. B Beam Interact. with Mater. Atoms. 166 (2000) 500–504. https://doi.org/10.1016/S0168-583X(99)00787-9.

[82] B. Macalik, Optical properties of gamma irradiated soda-lime silicate glasses exchanged with copper, Radiat. Eff. Defects Solids. 158 (2003) 403–406. https://doi.org/10.1080/1042015021000052340.

[83] R.K. Brow, Electron beam reduction of sodium-containing glass surfaces, J. Non. Cryst. Solids. 175 (1994) 155–159. https://doi.org/10.1016/0022-3093(94)90007-8.

[84] D.G. Howitt, H.W. Chan, J.F. DeNatale, J.P. Heuer, Mechanism for the Radiolytically Induced Decomposition of Soda–Silicate Glasses, J. Am. Ceram. Soc. 74 (1991) 1145–1147. https://doi.org/10.1111/j.1151-2916.1991.tb04358.x.

[85] A. Hassib, O. Beckman, H. Annersten, Photochromic properties of natural sodalite, J. Phys. D. Appl. Phys. 10 (1977) 771–777. https://doi.org/10.1088/0022-3727/10/5/018.

[86] J.C. Groote, J.R.W. Weerkamp, J. Seinen, H.W. Den Hartog, Radiation damage in NaCl. I. Optical-absorption experiments on heavily irradiated samples, Phys. Rev. B. 50 (1994) 9781–9786. https://doi.org/10.1103/PhysRevB.50.9781.

[87] E. Kolobkova, N. Nikonorov, Metal sodium nanoparticles in fluorophosphate glasses, J. Alloys Compd. 637 (2015) 545–551. https://doi.org/10.1016/j.jallcom.2015.02.148.

[88] E.S. Bochkareva, N. V. Nikonorov, O.A. Podsvirov, M.A. Prosnikov, A.I. Sidorov, The Formation of Sodium Nanoparticles in Alkali-Silicate Glass Under the Action of the Electron Beam and Thermal Treatments, Plasmonics. 11 (2016) 241–246. https://doi.org/10.1007/s11468-015-0046-8.

[89] J. Seinen, J.C. Groote, J.R.W. Weerkamp, H.W. Den Hartog, Radiation damage in NaC1. III. Melting phenomena of sodium colloids, Phys. Rev. B. 50 (1994) 9793–9797.

[90] J. Seinen, J.C. Groote, J.R.W. Weerkamp, H.W. Den Hartog, Radiation damage in NaC1. II. The early stage of F-center aggregation, Phys. Rev. B. 91 (1994). https://doi.org/10.1017/CBO9781107415324.004.

[91] J.C. Groote, J.R.W. Weerkamp, J. Seinen, H.W. Den Hartog, Radiation damage in NaCl. IV. Raman scattering, Phys. Rev. B. 50 (1994) 9798–9802. https://doi.org/10.1103/PhysRevB.50.9798.

[92] A. Wesełucha-Birczyńska, S. Zelek, K. Stadnicka, Blue halite colour centre aggregates studied by micro-Raman spectroscopy and X-ray diffraction, Vib. Spectrosc. 60 (2012) 124–128. https://doi.org/10.1016/j.vibspec.2011.11.001.

[93] H.S. Tsai, D.S. Chao, Y.H. Wu, Y.T. He, Y.L. Chueh, J.H. Liang, Spectroscopic investigation of gamma radiation-induced coloration in silicate glass for nuclear applications, J. Nucl. Mater. 453 (2014) 233–238. https://doi.org/10.1016/j.jnucmat.2014.07.002.

[94] N. Jiang, D. Su, J.C.H. Spence, S. Zhou, J. Qiu, Electron energy loss spectroscopy of Na in Na, Na_2O, and silicate glasses, J. Mater. Res. 23 (2008) 2467–2471. https://doi.org/10.1557/jmr.2008.0296.

[95] P. Mahadik, N. Pathak, P. Sengupta, Spectroscopic studies on blue halite, J. Lumin. 194 (2018) 327–333. https://doi.org/10.1016/j.jlumin.2017.10.013.

[96] A. Manara, M. Antonini, P. Camagni, P.N. Gibson, Radiation Damage in Silica-Based Glasses: Point Defects, Microstructural Changes and Possible Implications on Etching and Leaching., Nucl. Instruments Methods Phys. Res. Sect. B Beam Interact. with Mater. Atoms. 229 (B1) (1983) 475–480.

[97] J.O. Isard, The Mixed Alkali Effect in Glass, J. Non. Cryst. Solids. (1969) 235–261. https://doi.org/10.1111/j.1151-2916.1965.tb14784.x.

[98] Y. Tokuda, Y. Takahashi, H. Masai, S. Kaneko, Y. Ueda, S. Fujimura, T. Yoko, Local structure of alkalis in mixed-alkali borate glass to elucidate the origin of mixed-alkali effect, J. Asian Ceram. Soc. 3 (2015) 412–416. https://doi.org/10.1016/j.jascer.2015.09.002.

[99] J.F. DeNatale, D.K. McElfresh, D.G. Howitt, Preliminary observations on the microstructure of nuclear waste glasses, Ceram. Int. 8 (1982) 128–130. https://doi.org/10.1016/0272-8842(82)90002-5.

[100] N. Ollier, B. Boizot, B. Reynard, D. Ghaleb, G. Petite, β irradiation in borosilicate glasses: The role of the mixed alkali effect, Nucl. Instruments Methods Phys. Res. Sect. B Beam Interact. with Mater. Atoms. 218 (2004) 176–182. https://doi.org/10.1016/j.nimb.2003.12.014.

[101] J.F. Denatale, D.G. Howitt, The gamma-irradiation of nuclear waste glasses,

Radiat. Eff. 91 (1985) 89–96. https://doi.org/10.1080/00337578508222550.

[102] W.J. Weber, Radiation and Thermal Ageing of Nuclear Waste Glass, Procedia Mater. Sci. 7 (2014) 237–246. https://doi.org/10.1016/j.mspro.2014.10.031.

[103] B.F. Dunnett, Review of the Development of UK High Level Waste Vitrified Product (Nexia Solutions (06) 7926), (2007) 11–17.

[104] NDA, Geological Disposal An overview of the generic Disposal System Safety Case, 2010.

[105] B. Boizot, G. Petite, D. Ghaleb, B. Reynard, G. Calas, Raman study of beta-irradiated glasses, J. Non. Cryst. Solids. 243 (1999) 268–272.

[106] A. Abbas, Y. Serruys, D. Ghaleb, J.M. Delaye, B. Boizot, B. Reynard, G. Calas, Evolution of nuclear glass structure under α-irradiation, Nucl. Instruments Methods Phys. Res. Sect. B Beam Interact. with Mater. Atoms. 166 (2000) 445–450. https://doi.org/10.1016/S0168-583X(99)00695-3.

[107] H.D. Schreiber, A.L. Hockman, Redox Chemistry in Candidate Glasses for Nuclear Waste Immobilization, J. Am. Ceram. Soc. 70 (1987) 591–594. https://doi.org/10.1111/j.1151-2916.1987.tb05712.x

[108] O. Pinet, I. Hugon, S. Mure, Redox Control of Nuclear Glass, Procedia Mater. Sci. 7 (2014) 124–130. https://doi.org/10.1016/j.mspro.2014.10.017.

[109] L.D. Bogomolova, V.A. Jachkin, S.A. Prushinsky, S. V. Stefanovsky, Y.G. Teplyakov, F. Caccavale, EPR study of paramagnetic species in oxide glasses implanted with nitrogen, J. Non. Cryst. Solids. 220 (1997) 109–126. https://doi.org/10.1016/S0022-3093(97)00259-7

[110] V.I. Malkovsky, S. V. Yudintsev, M.I. Ojovan, V.A. Petrov, The Influence of Radiation on Confinement Properties of Nuclear Waste Glasses, Sci. Technol. Nucl. Install. 2020 (2020). https://doi.org/10.1155/2020/8875723.

[111] V. Pukhkaya, T. Charpentier, N. Ollier, Study of formation and sequential relaxation of paramagnetic point defects in electron-irradiated Na-aluminosilicate glasses: Influence of Yb, J. Non. Cryst. Solids. 364 (2013) 1–8. https://doi.org/10.1016/j.jnoncrysol.2013.01.021.

[112] C.P. Kaushik, Indian Program for Vitrification of High Level Radioactive Liquid Waste, Procedia Mater. Sci. 7 (2014) 16–22. https://doi.org/10.1016/j.mspro.2014.10.004.